The first electron beam polarization measurement with a diamond micro-strip detector

A. Narayan[1], D. Dutta[1], V. Tvaskis[2,3], D. Gaskell[4], J. W. Martin[2], A. Asaturyan[5], J. Benesch[4], G. Cates[6], B. S. Cavness[7], J. C. Cornejo[8], M. Dalton[6], W. Deconinck[8], L. A. Dillon-Townes[4], G. Hays[4], E. Ihloff[9], D. Jones[6], R. Jones[10], S. Kowalski[11], L. Kurchaninov[12], L. Lee[12], A. McCreary[13], M. McDonald[2], A. Micherdzinska[2], A. Mkrtchyan[5], H. Mkrtchyan[5], V. Nelyubin[6], S. Page[3], K. Paschke[6], W. D. Ramsay[12], P. Solvignon[4], D. Storey[2], A. Tobias[6], E. Urban[14], C. Vidal[9], P. Wang[3], and S. Zhamkotchyan[5]

[1]*Mississippi State University, Mississippi State, MS 39762, USA*
[2]*University of Winnipeg, Winnipeg, MB R3B 2E9, Canada*
[3]*University of Manitoba, Winnipeg, MB R3T 2N2, Canada*
[4]*Thomas Jefferson National Accelerator Facility, Newport News, VA 23606, USA*
[5]*Yerevan Physics Institute, Yerevan, 375036, Armenia*
[6]*University of Virginia, Charlottesville, VA 22904, USA*
[7]*Angelo State University, San Angelo, TX 76903, USA*
[8]*College of William and Mary, Williamsburg, VA 23186, USA*
[9]*MIT Bates Linear Accelerator Center, Middleton, MA 01949, USA*
[10]*University of Connecticut, Storrs, CT 06269, USA*
[11]*Massachusetts Institute of Technology, Cambridge, MA 02139, USA*
[12]*TRIUMF, Vancouver, BC V6T 2A3, Canada*
[13]*University of Pittsburgh, Pittsburgh, PA 15260, USA and*
[14]*Hendrix College, Conway, AR 72032, USA*

A diamond multi-strip detector was used for the first time, to track Compton scattered electrons in a new electron beam polarimeter in the experimental Hall C at Jefferson Lab. We report the first high precision beam polarization measurement with electrons detected in diamond multi-strip detectors. The analysis technique leveraged the high resolution of the detectors and their proximity to the electron beam ($\gtrsim$ 0.5 cm). The polarization was measured with a statistical precision of $<$ 1%/hr, and a systematic uncertainty of 0.59%, for a 1.16 GeV electron beam with currents up to 180 μA. This constitutes the highest precision achieved for polarization measurement of few-GeV electron beams.

PACS numbers:

INTRODUCTION

High precision nuclear physics experiments using polarized electron beams rely on accurate knowledge of beam polarization to achieve their ever improving precision. A parity violating electron scattering (PVES) experiment in the experimental Hall C at Jefferson Lab (JLab), known as the $Q_{\rm weak}$ experiment, is the most recent example [1, 2]. The goal of the $Q_{\rm weak}$ experiment is to measure the Standard Model parameter known as the weak mixing angle, at a low energy (relative to the Z^0 mass) with unprecedented precision. With a goal of $<$ 1% uncertainty, determination of electron beam polarization is one of the greatest technical challenges of the $Q_{\rm weak}$ experiment. The experiment utilized an existing Møller polarimeter [2, 3] and a new Compton polarimeter [2, 4] to monitor the electron beam polarization. The Compton polarimeter was the only polarimeter at JLab Hall C that could non-destructively monitor the beam polarization at very high beam currents. A novel aspect of this polarimeter was the first use of diamond detector technology for this purpose.

The use of *natural* diamond in the detection of charged particles and radiation has a long history; but the use of synthetic diamond grown through a process known as "chemical vapor deposition" (CVD) is a relatively recent development. Detailed reviews of diamond as charged particle detectors can be found in [12–14]. Thin sheets of centimeter-sized diamond are grown using the CVD process and the plates of diamond are then turned into charged particle detectors by depositing suitable electrodes on them [15].

Compared to the more commonly used silicon detector, the signal size in a diamond detector is smaller, but the higher electron and hole mobility of diamond leads to a faster and shorter duration signal. However, the well-established radiation hardness of diamond [16, 17] is by far the most important consideration for the use of diamond detectors in nuclear and particle physics experiments.

The use of Compton scattered electrons and/or back–scattered photons to measure the Compton asymmetry and thereby the electron beam polarization, is a well established polarimetry technique [5–10]. Most previous Compton polarimeters, other than the one used in the SLD experiment [7], relied primarily on detection of the scattered photons to measure the beam polarization. The SLD Compton polarimeter, which detected scat-

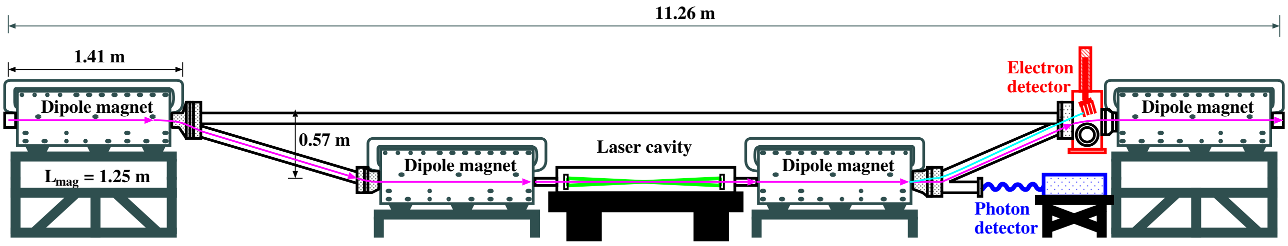

FIG. 1: Schematic diagram of the JLab Hall C Compton polarimeter.

tered electrons (and used detection of photons as a cross-check), was operated at a beam energy of 50 GeV and reported a precision of 0.5%. The relatively low energy of the electron beam at JLab leads to a smaller Compton analyzing power, and makes it significantly more challenging to achieve the same level of precision. Nonetheless, the Compton polarimeter in Hall A at Jefferson Lab has reported a relative precision of $\sim$ 1% by detecting the Compton scattered electrons at a beam energy of 3 GeV [11].

The JLab Hall C Compton polarimeter detects the scattered electrons in a set of tracking detectors. The low energy of the electron beam (1.16 GeV) and other operating parameters of the $Q_{\rm weak}$ experiment, presented the most challenging set of conditions to achieve the goal of $< 1\%$ uncertainty in measurement of the beam polarization. For example, it constrained the tracking detector to be placed as close as 0.5 cm from the electron beam. Further, the polarimeter was operated at the highest beam current (180 μA) ever used by any experiment at JLab and ran for over 5000 hrs, thereby subjecting the electron detectors to a rather large cumulative radiation dose ($>$ 100 kGy, just from electrons). In order to withstand the large radiation dose, a novel set of diamond micro-strip detectors were used to track the scattered electrons. In this letter we report the first high precision measurement of electron beam polarization with this device.

THE HALL C COMPTON POLARIMETER

A schematic of the Compton polarimeter in Hall C at JLab is shown in Fig. 1. It consists of four identical dipole magnets forming a magnetic chicane that displaces a 1.16 GeV electron beam vertically downward by 57 cm ($\sim$ 10.13 °). A high intensity ($\sim$ 1 - 2 kW) beam of $\sim$ 100% circularly polarized photons is provided by an external low-gain Fabry-Pérot laser cavity which consists of an 85 cm long optical cavity with a gain between 100 and 200, coupled to a green (532 nm), continuous wave, 10 W laser (Coherent VERDI). The laser light is focused at the interaction region ($\sigma_{\rm waist}$ $\sim$ 180 μm), and it is larger than the electron beam envelope ($\sigma_{\rm x/y}$ $\sim$ 40 μm when optimally tuned). The degree of circular polarization was determined by two methods; first by monitoring the polarization state of the transmitted laser light and using a transfer function to translate it to the Compton interaction point, and second, a more precise method of measuring the leakage of the back-reflected power from the laser cavity.

The laser was operated in $\sim$ 90 second cycles, where it is active for $\sim$60 s (laser on period) and blocked off (laser off period) for the rest of the cycle. The laser off data were used to measure the background. The helicity of the laser beam was reversed very infrequently (6 times during the entire experiment).

The maximum scattered photon energy was approximately 46 MeV. A calorimeter consisting of a 2 × 2 matrix of 3 cm × 3 cm $PbWO_4$ scintillating crystals attached to a single photo-multiplier tube was used to measure the scattered photon energy. The signal from the photon detector was digitally integrated with zero threshold over a full helicity state ($\sim$ 1 ms) using a 200 MHz flash analog to digital converter.

The Compton scattered electrons were momentum analyzed by the third dipole magnet of the chicane. The maximum separation between the primary electron beam and the Compton scattered electrons, just in front of the fourth dipole, was $\sim$ 17 mm. The deflection of the scattered electron with respect to the primary electron beam, from the maximum down to distances as small as $\sim$ 5 mm, was tracked by a set of four diamond micro-strip detectors. This range allowed the detection of a large fraction of the Compton electron spectrum, from beyond the kinematic maximum (strip 55 in Fig. 3) down past the zero-crossing point ($\sim$ 8.5 mm from the primary beam) of the Compton asymmetry. The electron detectors are made from 21 mm×21 mm×0.5 mm plates of CVD diamond [18]. Each diamond plate has 96 horizontal metalized electrode strips with a pitch of 200 μm (180 μm of metal and 20 μm of gap) on one side (front) and a single metalized electrode covering the entire diamond surface on the opposite (back) side. Details can be found in Ref. [2]. A photograph of a single detector plane is shown in Fig 2.

A typical charge normalized Compton electron spectrum, as well as a charge normalized background spectrum, is shown in Fig 3. A statistical precision of $< 1\%$ per hour was routinely achieved with these detectors. The observed Compton scattered electron rate, aggre-

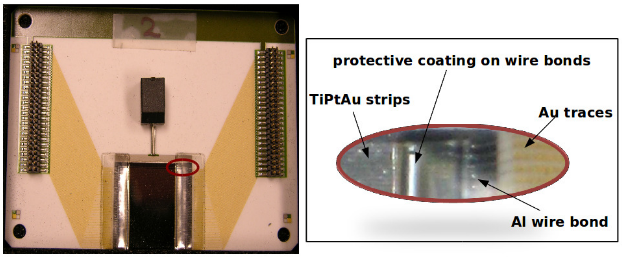

FIG. 2: A CVD diamond plate mounted on an alumina substrate which forms a single detector plane (left). The red oval indicates the area that has been shown in the enlarged view (right).

gated over all strips in each detector plane was ∼ 150–180 kHz. By comparing the expected to the observed rates, the detector efficiency was estimated to be ∼ 70%. The large separation between the detector and the read-out electronics was the leading cause of the inefficiency. The inter-strip fluctuations seen in Fig. 3 are due to strip-to-strip variation in the detector efficiency.

The data acquisition (DAQ) system employed a set of field programmable gate array (FPGA) based logic modules [19] to find clusters of detector hits, and to implement a track-finding algorithm, which generated a trigger when the same cluster was identified in multiple active planes. The size of the cluster was defined as 4 adjacent strips. Only 3 detector planes were operational during the experiment and the typical trigger condition was set to 2 out of 3 planes.

Over the 2 year period of the Q_{weak} experiment, the detectors were exposed to a radiation dose of ∼ 100 kGy (without including the dose from Synchrotron radiation). No significant degradation of the signal size was observed during this period, demonstrating the radiation hardness of the diamond detectors.

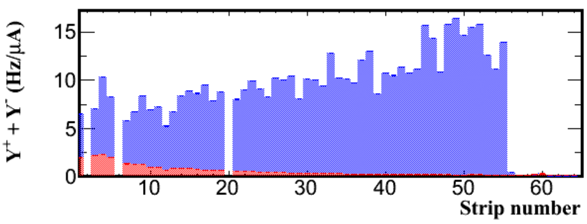

FIG. 3: A typical spectrum of normalized yield $(Y^+ + Y^-)$ from the detector strips for a single detector plane. The charge normalized background subtracted spectrum is shown in blue and the charge normalized background is shown in red.

DATA REDUCTION AND RESULTS

The electron beam helicity was reversed at a rate of 960 Hz in a pseudo-random sequence. In addition a half-wave plate in the polarized electron photo emission source [20] was inserted or removed about every 8 hours to reverse the beam helicity relative to the polarization of the source laser. The background yield measured during the laser-off period was subtracted from the laser-on yield for each electron helicity state, and a charge normalized Compton yield for each detector strip was obtained for the two electron helicities (as shown in Fig. 3). The measured asymmetry was built from these yields using,

$$A_{exp} = \frac{Y^+ - Y^-}{Y^+ + Y^-}, \tag{1}$$

where $Y^{\pm} = \frac{N^{\pm}_{on}}{Q^{\pm}_{on}} - \frac{N^{\pm}_{off}}{Q^{\pm}_{off}}$ is the charge normalized Compton yield for each detector strip, $N^{\pm}_{on/off}$ and $Q^{\pm}_{on/off}$ are the detector counts and the beam charge accumulated during the laser on/off period for the two electron helicity states (±), respectively. The Compton yields were integrated over two different time intervals, ∼250 thousand helicity cycles and 1 laser cycle. The asymmetries extracted over both time intervals, and averaged over an hour long run, were consistent with one another. A typical spectrum for an hour long run is shown in Fig. 4. The background asymmetry is consistent with zero within the statistical uncertainties, and given the large signal-to-background ratio of 5–20 (see Fig. 3) the dilution to the measured asymmetry due to the background is negligible.

The electron beam polarization P_e was extracted by fitting the measured asymmetry to the theoretical Compton asymmetry using;

$$A_{exp}(y_n) = P_e P_\gamma A_{th}(y_n), \tag{2}$$

where P_γ is the polarization of the photon beam, y_n is the scattered electron displacement along the detector plane for the n-th strip, and A_{th} is the $\mathcal{O}(\alpha)$ theoretical Compton asymmetry for fully polarized electrons and photon beams. The radiative corrections to the Compton asymmetry were calculated to leading order within a low energy approximation applicable for few GeV electrons [21]. The relative change in the Compton asymmetry due to radiative corrections was <0.3%.

The quantity A_{th} is typically calculated as a function of the dimensionless variable $\rho = E_\gamma / E_\gamma^{max}$, where E_γ and E_γ^{max} are the energy of the back-scattered photon and its maximum value, respectively. In order to directly compare with the measured asymmetry, ρ was mapped, by a third order polynomial, to the displacement of the scattered electron along the detector plane y_n. Further, y_n is linearly related to detector strip number, and depends on several parameters, such as, dimensions and dispersion of the chicane magnets, and exact location of the detectors with respect to the third dipole.

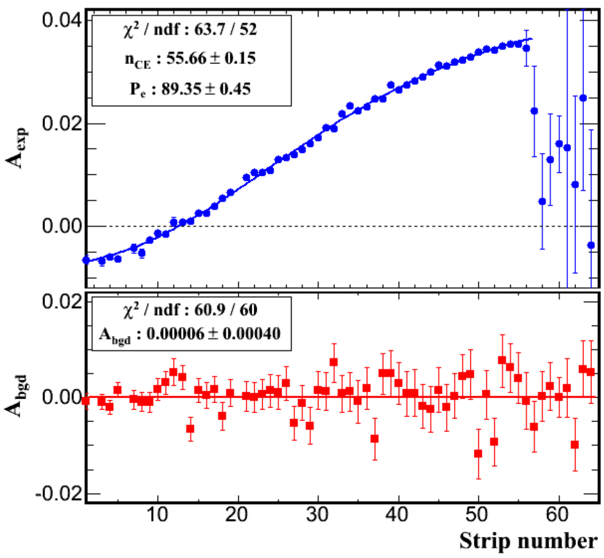

FIG. 4: The measured asymmetry as function of detector strip number for a single detector plane during the laser-on period (top) and the background asymmetry from the laser-off period (bottom). The strip number is linearly mapped to the displacement of the scattered electron from the primary beam. The dashed line in the top panel corresponds to $A_{exp} = 0$. The solid blue line (top) is a fit to Eq. 2 and the solid red line (bottom) is a fit to a constant value. Only statistical uncertainties are shown in this figure.

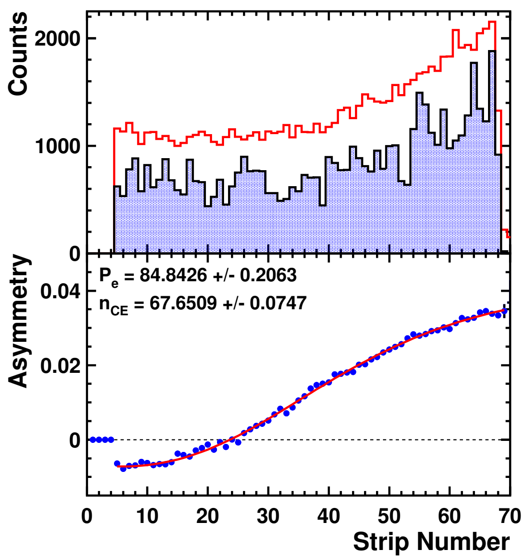

FIG. 5: (top) A typical Monte Carlo simulated Compton spectrum for a single detector plane, with (blue, shaded) and without (red) detector inefficiency. The counts have been scaled by a factor of 10^{-3}. (bottom) The Compton asymmetry extracted from the simulated spectrum including detector inefficiency (blue circles), and a two parameter fit to the calculated asymmetry (red line). The input asymmetry was 85%.

The measured asymmetry A_{exp} was fit to Eq. 2 for each detector strip, with P_e and n_{CE} as the two free parameters. The number of degrees of freedom was typically between $50 - 60$, which was made possible by the high resolution of the detector, and the proximity of the detector to the primary electron beam. The detection of a large fraction of the Compton electron spectrum, spanning both sides of the zero crossing of the Compton asymmetry, significantly improved the robustness of the fit and the analysis technique. A typical fit is shown in Fig. 4. The χ^2 per degree-of-freedom of the fit ranges between $0.8 - 1.5$ for all production runs reported here.

A Monte Carlo (MC) simulation of the Compton polarimeter was coded in the Geant3 [22] detector simulation package. In addition to Compton scattering, the simulation included backgrounds from beam-gas interactions and beam halo interactions in the chicane elements. The simulation also incorporated the effects of detector inefficiency, the track-finding trigger, and electronic noise. A typical simulated strip-hit spectrum (with and without detector inefficiency), and the asymmetry extracted from simulated spectra are shown in Fig. 5. The simulation was used to validate the analysis procedure and to study a variety of sources of systematic uncertainties. For each source, the relevant parameter was varied within the expected range of uncertainty, and the change in the extracted polarization was listed as its contribution to the systematic uncertainty. The list of contributions is shown in Table I.

The MC simulation demonstrated that secondary particles knocked out by the Compton scattered electron passing through the first plane produced a 0.4% change in polarization in the subsequent planes, consistent with observation. A correction for the second and third planes could be made but at the cost of a slightly higher systematic uncertainty, and hence only the results from the first detector plane are quoted here.

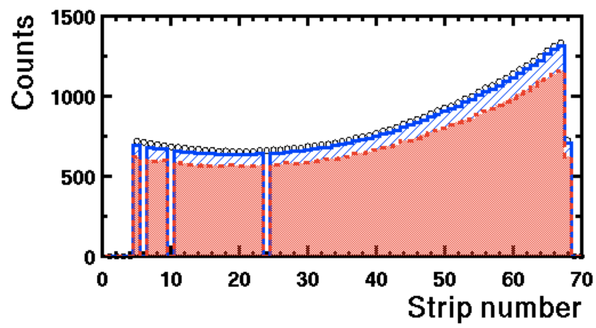

FIG. 6: A typical Modelsim simulated spectrum (without noise and detector inefficiency) of a single detector plane, for un-triggered (blue solid, diagonally hatched) and triggered (red dashed, shaded) DAQ modes. The input spectrum is shown as the black open circles. The counts have been scaled by a factor of 10^{-3}. The missing strips correspond to very noisy strips that were masked in the DAQ system.

There were several sources of inefficiency associated with the DAQ system, such as the algorithm used to identify electron tracks and form the trigger, and the dead-time due to a busy (hold off) period in the DAQ. The entire DAQ system was simulated on a platform called Modelsim [23]. While in Monte Carlo simulations, events are generated based on the probability distribution for the relevant physics process, in contrast Modelsim is a simulation technique based on time steps. It employs the same firmware, written in the hardware description language for very high speed integrated circuits (VHDL), that operated the logic modules in the DAQ system. The DAQ simulation included signal generators that mimic the electron, the background and the noise signals, along with a detailed accounting of delays due to the internal signal pathways in the logic modules and the external electronic chain. Fig. 6 shows the output spectra from a Modelsim simulation, for the triggered and the un-triggered modes, along with the input spectrum. Noise and detector inefficiencies were not included in these simulations as they were shown to have minimal impact on the determination of the DAQ inefficiencies. The small difference between the input and the un-triggered counts is a result of the DAQ being disabled during helicity reversal. The difference between the triggered and the un-triggered counts is due to DAQ inefficiency. The average DAQ inefficiency was found to be directly related to the aggregate detector rate.

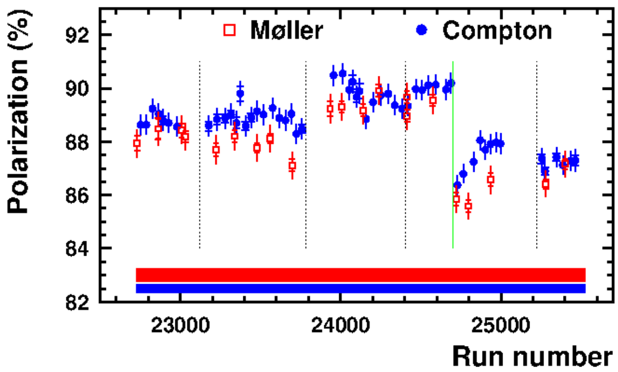

FIG. 7: The extracted beam polarization as a function of run-number averaged over 30 hour long periods, during the second run period of the Q_{weak} experiment (blue, circle). Also shown are the results from the intermittent measurements with the Møller polarimeter [2, 3] (red, open square). The inner error bars show the statistical uncertainty while the outer error bar is the quadrature sum of the statistical and point-to-point systematic uncertainties. The solid bands show the additional normalization/scale type systematic uncertainty. The dashed and solid (green) vertical lines indicate changes at the electron source.

The DAQ simulation was used to determine the correction to the detector yield for each 1 hr run, based on the aggregate detector rate during the run. The DAQ inefficiency correction resulted in < 1% change in the extracted polarization. The validity of the corrections and the systematic uncertainty due to the corrections (listed in Table I) was determined by comparing the polarization extracted from triggered vs. un-triggered data over a wide range of beam currents (rates) and several different trigger conditions. Thus, the Modelsim simulation provided a robust method to determine the inefficiency of the DAQ.

TABLE I: Systematic Uncertainties

Source	Uncertainty	$\Delta P/P\%$
Laser Polarization	0.18	0.18
Plane to Plane	secondaries	0.00
magnetic field	0.0011 T	0.13
beam energy	1 MeV	0.08
detector z position	1 mm	0.03
inter plane trigger	1-3 plane	0.19
trigger clustering	1-8 strips	0.01
detector tilt(w.r.t x, y and z)	1 degree	0.06
detector efficiency	0.0 - 1.0	0.1
detector noise	up to 20% of rate	0.1
fringe field	100%	0.05
radiative corrections	20%	0.05
DAQ inefficiency correction	40%	0.3
DAQ inefficiency pt.-to-pt.		0.3
Beam vert. pos. variation	0.5 mrad	0.2
helicity correl. beam pos.	5 nm	< 0.05
helicity correl. beam angle	3 nrad	< 0.05
spin precession in chicane	20 mrad	< 0.03
Total		0.59

Extensive simulation studies provided the comprehensive list of contributions to the systematic uncertainties, tabulated in Table I, with a net systematic uncertainty of 0.59% for the Compton Polarimeter. The extracted beam polarization for the entire second running period of the Q_{weak} experiment is shown in Fig. 7. Most of the variation in the polarization are due to changes at the electron source indicated by the dashed and solid (green) vertical lines. The Compton and Møller measurements [2, 3] were quantitatively compared by examining periods of stable polarization. The ratio of Compton to Møller measurements, when averaged over these stable periods using statistical and point-to-point uncertainties, was found to be 1.007 ± 0.003.

CONCLUSIONS

The polarization of a 1.16 GeV electron beam was measured using a set of diamond micro-strip detectors for the first time. The high resolution of the detectors and their proximity to the primary beam helped record a large fraction of the Compton electron spectrum, spanning both sides of the zero crossing of the Compton asymmetry. These detectors, coupled with a robust analysis technique and rigorous simulations of the polarimeter and the DAQ system, produced a very reliable, high precision measurement of the polarization in a very high radiation environment. They demonstrate that diamond micro-strip detectors are indeed a viable option as tracking detectors, and they are the appropriate choice for tracking detectors that are exposed to very high radiation dose. We have also demonstrated that it is possible to achieve high precision with a Compton polarimeter operated at beam energies as low as ~ 1 GeV. This has very positive implications for the future PVES program at the upgraded JLab.

ACKNOWLEDGMENTS

This work was funded in part by the U.S. Department of Energy contract # AC05-06OR23177, under which Jefferson Science Associates, LLC operates Thomas Jefferson National Accelerator Facility, and contract # DE-FG02-07ER41528, and by the Natural Sciences and Engineering Research Council of Canada (NSERC). We thank H. Kagan from Ohio State University for teaching us about diamonds, training us on characterizing them and helping us build the proto-type detector.

[1] D. Androic *et al.*, Phys. Rev. Lett. **111**, 121804 (2013).
[2] T. Allison *et al.*, Nucl. Instr. Meth. **A781**,105 (2015).
[3] J. Magee, Proc. of Sci. PSTP2013, 039 (2013).
[4] A. Narayan, Ph. D. Thesis, Mississippi State University, 2015 (unpublished).
[5] D. Gustavson *et al.* Nucl. Instr. Meth. **A165**, 177 (1979); L. Knudsen *et al.*, Phys. Lett. **B270**, 97 (1991).
[6] D. P. Barber *et al.*, Nucl. Instr. Meth. **A329**, 79 (1993).
[7] M. Woods, Proc. of the Workshop on High Energy Polarimeters, Amsterdam, eds. C. W. de Jager et al., p. 843 (1996); SLAC-PUB-7319 (1996).
[8] I. Passchier *el al.*, Nucl. Instr. Meth. **A414**, 446 (1998).
[9] W. Franklin *et al.*, AIP Conf.Proc. 675, 1058 (2003).
[10] M. Baylac *et al.*, Phys. Lett. **B539**, 8 (2002); N. Felletto *et al.*, Nucl. Instr. Meth. **A459**, 412 (2001).
[11] A. Acha *et al.* [HAPPEX Collaboration], Phys. Rev. Lett. **98**, 032301 (2007).
[12] D. R. Kania, M. I. Landstrass and M. A. Plano, Diam. Relat. Mater. **2**, 1012 (1993).
[13] R. Berman (ed), *Physical Properties of Diamond*, Oxford University Press, Oxford, 1965.
[14] J. E. Field (ed), *The Properties of Diamond*, Academic, New York, 1979.
[15] R. J. Tapper, Rep. Prog. Phys. **63**, 1273 (2000).
[16] C. Bauer *et al.* Nucl. Instrum. Methods **367**, 207 (1995).
[17] M. M. Zoeller *et al.*, IEEE Trans. Nucl. Sci. **44** 815 (1997).
[18] The CERN grade diamond plates were procured from Element Six, 35 West 45th St., New York, NY 10036, USA.
[19] V1495 modules from CAEN Technologies, Inc. 1140 Bay Street, Suite 2C, Staten Island, NY 10305 - USA
[20] C.K. Sinclair *et al.*, Phys. Rev. ST Accel. Beams **10**, 023501 (2007); P.A. Adderley *et al.*, Phys. Rev. ST Accel. Beams **13**, 010101 (2010).
[21] A. Denner and S. Dittmaier, Nucl. Phys.**B540**, 58 (1999).
[22] CERN Program Library Long Write-up W5013, Unpublished (1993)
[23] Modelsim Reference Manual, Mentor Graphics Corp.,Unpublished (2010).